Redshift evolution of baryon fraction and formation of massive galaxy clusters using MACSIS simulations

William Cooper
The University of Manchester
Department of Physics and Astronomy

Supervisor: Dr Scott Kay
Project collaborator: Aaron Callaghan
(Dated: November 6, 2023)

Using the MAssive ClusterS and Intercluster Structures (MACSIS), N-body simulations, in which realistic large galaxy clusters are produced, the redshift evolution of galaxy cluster formation and properties can be studied. For every massive galaxy cluster, the FoF algorithm split the cluster into separate defined objects. The primary candidate is the most massive progenitor on which every MACSIS zoom simulation is centred, and secondary candidates represent smaller objects inside the cluster. Creating a candidate catalogue for each MACSIS cluster including the primary candidate and secondaries, at every redshift, was a big part of this project. The catalogue allowed the study of the majority of the work done in this paper by allowing analysis of smaller objects inside the cluster and has built a foundation for future work on MACSIS clusters. We study the formation of galaxy clusters by using secondary candidate statistics. This involves tracking secondary candidates' mass and distance to the centre of the cluster to track the breakup of objects with increasing redshift. Our results show that MACSIS successfully simulates hierarchical structure formation in massive galaxy clusters using this method. The main galaxy cluster property of interest is the baryon fraction. Massive galaxy clusters are so large they represent the universal baryon fraction, so the study of the redshift evolution of baryon fraction inside massive clusters provides benefits to understanding the change in the baryon fraction of the universe at different time frames. We calculate the total baryon fraction and the hot baryon fraction, which contains hot gas of above $10^6 K$, to represent all the baryonic content and just the observation X-ray emitting baryonic content. We find both baryon fractions strongly depend on candidate mass, especially at z = 0, and that candidates with smaller masses consist of a high fraction of cold gas. The trend of total baryonic matter decreases with decreasing redshift, alongside the constant trend of hot baryon fraction both agree with observational data. Furthermore, the decrease of baryon fraction occurring at a faster rate for low-mass objects inside galaxy clusters also agree with data from another simulation. Moreover, by using the hot baryonic gas fraction divided by the total baryonic fraction we theoretically calculated the missing baryon fraction that would occur observationally due to non-X-ray emitting gas. Low mass candidates have a much higher missing baryonic component due to the high cold gas content. Massive candidates have basically no missing baryonic component at z = 0, further suggesting they have an extremely little cold gas percentage. Even the baryonic fraction of the most massive primary candidates doesn't equal the universal baryon fraction $\overline{f_b} = \frac{\Omega_b}{\Omega_m} = 0.157$. However, by increasing the radius of which the total baryonic fraction is calculated, the deficit of baryonic fraction goes from 10 percent to 1 percent at five times the virial radius (R_{200}). The finding of baryon matter on the outskirt of the halo agrees with observational data at z = 0.

I. INTRODUCTION

Galaxy clusters are bound, high-density systems of galaxies, held together by their own gravity (Bahcall 1996). They are developed from primordial density fluctuations, which over time have collapsed and virialised to their current state (Barnes et al. 2017). The origin of these fluctuations can be explained via the universally-accepted Λ-Cold Dark Matter (ΛCDM) model, which is a hierarchical method of structuring or 'bottom-up' scenario (Diemand et al. 2011; Efstathiou et al. 1988; Houjun Mo et al. 2010). Therefore, using the redshift evolution of galaxy clusters and the ΛCDM model, we can probe the structures for galaxy formation in MACSIS. Furthermore, since the dynamical timescales of galaxy clusters are similar to the age of the universe, clusters reserve a footprint of their formation (Mushotzky 1998; Huss et al. 1999).

Galaxy clusters are the most massive virialized systems in the universe (Rasheed et al. 2011) and are constituents of the large-scale structure of the universe. For instance, the nodes of the filaments in the cosmic web (Bond et al. 1996). The large mass clusters used in this paper via MACSIS cover large regions of approximately $\sim 10 Mpch^{-1}$ and therefore can be assumed to be representative of the mean matter content of the universe (Rasheed et al. 2011). Furthermore, the deep gravitational potential wells of these galaxy clusters imply that baryonic matter cannot easily break free via feedback processes of the cluster (Barnes et al. 2017). Thus, the galaxy clusters can be assumed to

maintain the universal baryon fraction (Rasheed et al. 2011).

The MAssive ClusterS and Intercluster Structures (MACSIS) project provides a sample of 390 realistic massive galaxy clusters with $M_{FoF} > 10^{15} M_{\odot}$ selected from a large volume dark matter parent simulation and further re-simulated with full gas physics. Previously the BAHAMAS simulation was run on this parent simulation, but due to computational constraints at the time, the volume regions were too small to include clusters over $M_{FoF} > 10^{15} M_{\odot}$. The zoom simulations of the MACSIS project provides an extension to the BAHAMAS simulations to the most massive clusters possible via the ΛCDM model, allowing more observations across a range of cluster masses (Barnes et al. 2017).
The Friends-of-Friends (FoF) algorithm can be used to define galaxy haloes. The algorithm connects simulated particles to create networks known as FoF groups or haloes (More et al. 2011; Davis et al. 1985). In each individual one of the 390 selected clusters, using the FoF algorithm, a list of FoF haloes is produced. Now a catalogue of candidates can further be created from this. The primary candidates are defined as the most massive progenitor (most mass) in the FoF group, everything else in the FoF group is defined as a secondary candidate if it meets the criteria described in section 2. For each cluster, the unique halo region id of the cluster is saved alongside the primary candidate and all secondary candidates for said region. This catalogue provides valuable information for this paper and further work.

In this paper, these two properties, galaxy structure and baryon fraction will be analysed in detail via primary and secondary candidates of each MACSIS cluster at a range of redshifts. Galaxy structure for different redshift can provide validity of galaxy formation models such as ΛCDM, and calculating the baryon fraction can be used to understand processes such as accretion and feedback earlier in the universe. Both are also useful to provide possible insight into real-world observations of high redshift galaxy clusters when the technology becomes available.
The baryon fraction calculations were extended to just include hot gas ($> 10^6 K$), this is to simulate X-ray observations which are carried out in the real world. This can then be used to calculate the percentage of the baryons that would not be observed and how the resulting baryon fraction would change for different mass ranges. The baryon fraction for across all candidates were also below the universal value created during the big bang. To find these missing baryons the current radius used to calculate the baryon fraction within was extended.

The paper is organised as follows. Section 2 consists of the theory of galaxy clusters and their formation alongside significant processes that occur within them that may explain our results. MACSIS is also covered in more detail, specifically how clusters are selected. In Section 3 there is more detail about the candidate catalogue as well as the selection criteria for the candidates. Then the results are divided into candidate statistics and baryon fraction calculations in Section 4. Finally, Section 5 is the conclusion which summarises the produced results.

II. THEORY AND SIMULATIONS

A. Galaxy Clusters

Galaxy clusters are the largest gravitationally bound and virialized structures in the universe (Rasheed et al. 2011). When a system of gravitational interacting particles has become stable the system is virialized, however, the substructures inside the system may still interact between themselves but the system itself does not expand or collapse. Clusters of galaxies are constituents of the cosmic web filaments and as a result, clusters are not isolated systems (Kaastra et al. 2008). Between clusters is the Warm-Hot Intergalactic Medium (WHIM) that makes up the remainder of the cosmic filaments. This fundamental nature of matter to come together from atoms forming molecules to galaxies forming clusters is intriguing and galaxy clusters seem to be the top of the chain (Gorenstein et al. 1978). The three major components of galaxy clusters are hundreds to thousands of galaxies consisting of stars, gas and dust, the hot, X-ray emitting gas known as the Intra-Cluster Medium (ICM) and finally dark matter (Chandra X-ray observatory 2012).

In large galaxy clusters, the composition of the baryonic matter mostly lies within the ICM even despite its very low density and low mass fraction of the cluster mass (Lisa Germany et al. 1999). The ICM is heated up via processes discussed in subsection 1. This hot gas is in quasi-hydrostatic equilibrium within the dark matter-dominated gravitational potential well of the galaxy cluster (Kaastra et al. 2008). Quasi-hydro-static equilibrium is achieved if a system has a balance between the gravity gradient and pressure gradient. The hot gas emits X-ray emission primarily via bremsstrahlung emission, assuming the gas is composed of mostly hydrogen (Sarazin 1988; Houjun Mo et al. 2010), which is a primary method to make observations of clusters from Earth.

As mentioned, dark matter is needed to keep the hot gas inside the cluster in equilibrium. Individual galaxies and galaxy groups/clusters are embedded in a massive distribution of dark matter. Evidence for this dark matter is the

velocity rotational curves of galaxies, the velocity stays constant at increasing radii giving a need for this invisible mass. This dark matter structure is known as a dark matter halo, they are an essential part of the current cosmological model Taylor 2011, the ΛCDM model. Further discussed in subsection 2.

The results calculated in MACSIS often have units in R_{200} and M_{200} for distances and masses involved with clusters, respectively. R_{200} is defined as the radius at which the cluster's average enclosed density is two hundred times that of the universe's critical density (Barnes et al. 2017). M_{200} is the combined mass of all particles within R_{200}. The equation to show this is as follows,

$$M_{200} = 200\rho_{cr}(z)\frac{4}{3}\pi(R_{200})^3, \tag{1}$$

where ρ_{cr} is the critical density of the universe as a function of redshift (z) as the ρ_{cr} changes over time. R_{200} is also known as the virial radius.

1. Processes

Non-gravitational processes that occur inside galaxy clusters and the galaxies themselves have a significant impact on galaxies and galaxy clusters such as their evolution and current properties. Star formation, radiative cooling and feedback by Active Galactic Nuclei (AGN) are amongst the most critical processes simulated in MACSIS (Barnes et al. 2017; Eckert et al. 2021; Houjun Mo et al. 2010). Simulations that have included AGN feedback provide evidence that it is critically important to reproduce many cluster properties (Barnes et al. 2017). Supermassive black holes are accountable for many of the processes talked about here, they are thought to be positioned at the centre of many galaxies (Lisa Germany et al. 1999), therefore, galaxy clusters have an abundance of them. AGNs are responsible for the bright nuclei of galaxies, they produce the full range of the electromagnetic spectrum, and are powered by the accretion of matter (mostly gas) onto the supermassive black hole (Lisa Germany et al. 1999; Padovani et al. 2017). Black holes lay dormant until an influx of gas or a merger excites it and the AGN. Since star formation requires cold gas, star formation activity can be correlated to AGN activity. Furthermore, AGN can be said to regulate star formation, and as an extension galaxy evolution, as the gas can be stripped from the galaxy by the AGN. The interaction of AGN and the surrounding environment provide clues of evolution via black hole growth (Bufanda et al. 2016). For example, it is known that galaxies in clusters show very little star formation compared to isolated galaxies, this is because they evolve at different rates due to the high-density environment clusters exhibit and the physical processes that come with it such as ram pressure stripping, galaxy strangulation and galaxy harassment (Bufanda et al. 2016; Lisa Germany et al. 1999). This idea of galaxy evolution dependency on its environment can be observed from the morphology density relation, where early-type galaxies are often found in galaxy clusters whilst late-type galaxies are found in lower-density environments (Lisa Germany et al. 1999). This relation would infer that high-density environments, such as galaxy clusters, reduce the evolution of galaxies which can be explained by the processes just mentioned.

The ICM, as previously mentioned, is very hot and a strong X-ray emitter. The ICM was at first strange to astronomers due to its heat, as they thought it would have radiatively cooled down to ignite more star formation and make more galaxies. However, when the gas in the ICM cools down it falls to the cluster centre and is accreted by AGN of active galaxies. The interaction of accreted matter and the black hole releases a galactic jet, containing a lot of high-energy particles. This jet extends outside the galaxy back into the ICM, heating up the cluster gas and stopping the inflow of cold gas to the AGN. But the gas cools down again and the cycle repeats, this is known as the AGN feedback loop (Lisa Germany et al. 1999; Eckert et al. 2021).

Another consequence of AGN feedback is the displacement of baryonic matter, lowering the baryonic fraction of galaxies and galaxy groups. Galaxy cluster haloes are thought to retain all baryons due to their immense size and mass. However, AGN feedback still has enough energy to displace the baryons to larger radii (beyond virial radius) resulting in a low baryon fraction at small radii (Eckert et al. 2021).

2. Formation

A cosmological model is a method to try to understand large-scale structures of the universe, such as galaxy clusters, and allows the opportunity to study evolution and structure (Ellis 2006). The 'standard' cosmological model is widely accepted to be the Λ-Cold Dark Matter (ΛCDM) model due to its success in recreating the most realistic universe in simulations such as MACSIS. This model suggests the universe contains a low percentage (5 percent) of baryonic matter that is dominated by two dark components, Cold Dark Matter (CDM) and dark energy denoted as Λ (Taylor 2011). The large-scale structures follow the CDM components of the model (Diemand et al. 2011). It is

proposed CDM consists of Weakly Interacting Massive Particles (WIMPs), and candidates of such particles include light superpartners derived from an extension of the standard model known as super-symmetry (Jungman et al. 1996). Many experiments are underway to search for the undiscovered WIMPS.

The ΛCDM model is characterised by a hierarchical structure formation also known as bottom-up scenario (Diemand et al. 2011; Efstathiou et al. 1988; Houjun Mo et al. 2010), the formation of the larger structure by the merging of smaller ones via the gravitational interaction of particles (White et al. 1991). In the CDM models, massive haloes are a consequence of mergers of many small haloes (Houjun Mo et al. 2010). The cold part in ΛCDM model refers to the low thermal velocities of dark matter particles to allow small structures, such as microhaloes, to form which are the smallest and first objects to form in the universe under this model (Anderhalden et al. 2013). During the universe's inflationary stage, small perturbations were present due to quantum fluctuations. These perturbations can be observed via temperature fluctuations in the Cosmic Microwave Background (CMB) (Vikhlinin et al. 2014). These primordial fluctuations cause localised overdensities leading to gravitational collapse to form small structures. Further merging of small objects creates larger structures, a hierarchical mechanism, to get galaxy clusters. This merging process is stopped when the object created is virialised (Kaastra et al. 2008). The CDM model represents a flat universe, this provides the necessary cosmological parameters for the hierarchical structure formation of galaxy clusters to occur at the current epoch (Huss et al. 1999). The time taken to build galaxy clusters depends on how much dark matter is present in the universe, whether it is hot (Hot Dark Matter model), cold (CDM) or a mix (Hot-Cold Dark Matter model) alongside if the universe is flat, open and expanding (Huss et al. 1999; Chandra X-ray observatory 2012).

3. Mass Fractions

Mass fractions involve baryon, gas (hot and cold) and star fraction to study a range of phenomena such as understanding processes that can affect the baryon fraction depending on mass and redshift, star formation in different mass clusters using the star fraction, as well as the missing baryon fraction that occurs observationally at redshift 0.

In the current popular cosmological model, the Λ-Cold Dark Matter (ΛCDM) model as previously mentioned in the Formation subsection, baryonic matter only makes up roughly 5 percent of the universe. Baryonic matter are the constituents that make up visible matter, such as quarks and electrons and out of which galaxies and galaxy clusters are made (Houjun Mo et al. 2010). However, at higher redshifts ($z > 3$) most of the universal baryonic content can be accounted for, but at low redshifts, half of the baryons are missing observationally. We know the majority of observed baryons at lower redshifts lie within the ICM and Inter-Galactic Medium (IGM) and not in stars due to processes explained in the Processes subsection but there still remains baryons unaccounted for (Houjun Mo et al. 2010; Lisa Germany et al. 1999). It is thought that the gas could be heated to $(10^5 - 10^6 K)$ which makes it very difficult to detect (Houjun Mo et al. 2010). Using MACSIS, as there is no such observational difficulty, we can calculate the missing baryon fraction that observations may miss due to temperature using the difference in the hot and cold gas.

Using MACSIS, the baryon fraction is calculated using the mass ratio of star and gas particles divided by star, gas and dark matter particles within R_{200} of a candidate given by equation 2. The universal baryon mass fraction used in the MACSIS simulation is $\overline{f_b} = \frac{\Omega_b}{\Omega_m} = \frac{0.04825}{0.307} = 0.157$, where Ω_b and Ω_m are cosmological parameters describing the baryon fraction and the total mass fraction respectively. The total baryon faction (hot and cold gas) is given by:

$$f_b = \frac{M_{gas} + M_{stars}}{M_{gas} + M_{stars} + M_{darkmatter}} = \frac{M_{gas} + M_{stars}}{M_{200}}, \tag{2}$$

where the M of each particle type is the summed mass of all that particle type within a spherical volume of radius R_{200}, hence why the denominator can be assumed to be M_{200} by using equation 1. The hot baryon fraction is calculated by just using M_{gas} of particles above the temperature threshold $(\geq 10^6 K)$:

$$f_{b,hot} = \frac{M_{gas}(\geq 10^6 K) + M_{stars}}{M_{200}}. \tag{3}$$

B. MACSIS

The parent simulation of MACSIS is a periodic cube with a volume of $(3.2Gpc)^3$. The volume of the simulation was chosen to ensure it would contain a population of massive galaxy clusters. The parent simulation and MACSIS are N-body simulations, a simulation of N particles or objects and their motion subject to particle-particle interactions. In N-body simulations, the motion of each individual particle, such as gas, stars and dark matter, is calculated using

gravitational forces exerted on the said particle by every other particle in the system. Using this technique each particle in the system can be studied in how it interacts with others over time and how the whole system evolves, in this case, galaxy clusters. At such large volumes, it is currently too computationally expensive to simulate it using full gas physics, hydrodynamics and processes mentioned in the processes subsection, at a high enough resolution to calculate properties interested in. Instead, the parent simulation was run with only dark matter particles from redshift z=127 to current z=0, this still produces a realistic result as dark matter and its gravitational presence was dominant in the formation and evolution of large-scale structures in the universe as mentioned in the theory subsection (Diemand et al. 2011). The simulation contained N = 2520^3 dark matter particles with mass $m_{DM} = 5.43 \times 10^{10} M_{\odot} h^{-1}$. All masses and distances are presented in comoving coordinates (h^{-1}), in this simulation Hubble's constant $h = 0.6777$ (Barnes et al. 2017).

At z=0 networks of particles, representing the dark matter haloes of galaxy clusters, were identified using the Friends-of-Friends (FoF) algorithm (Davis et al. 1985). The algorithm links two particles if the separation distance between them is less than the linking length $b\bar{l}$, where $\bar{l}$ is the mean inter-particle distance in the simulation and b is a free parameter given a value of 0.2 (Barnes et al. 2017; More et al. 2011; Davis et al. 1985). If particles are closer than the linking length, the algorithm connects them to build a network of particles known as FoF haloes. The list of FoF haloes is ordered in descending mass. Further work involved with refining the FoF haloes list is described in the Candidate Catalogue subsection.

To select the haloes of the MACSIS sample, from the dark matter-only parent simulation, all haloes with $M_{FoF} > 10^{15} M_{\odot}$ were divided in logarithmically spaced bins of width $\Delta log_{10} M_{FoF} = 0.2$. A maximum of 100 haloes were chosen from each bin, if a bin contained more the haloes were further subdivided and then selected randomly to remove any bias (Barnes et al. 2017). This selection procedure produced 390 haloes, which will be the basis for MACSIS.

Previously the BAHAMAS simulation was run on this parent simulation, but due to computational constraints at the time, the volume regions were too small to include clusters over $M_{FoF} > 10^{15} M_{\odot}$. The zoom simulations of the 390 haloes in MACSIS provide an extension to the BAHAMAS simulations to the most massive clusters possible via the ΛCDM model, allowing more observations across a range of cluster masses. The zoom simulation technique is to re-simulate the same sample at greater resolution, to include full gas physics and dark matter only simulations, to solve for hydrodynamical/gravitational and gravitational aspects respectively (Barnes et al. 2017). However, processes mentioned in the processes subsection occur on too small of a scale that still cannot be resolved due to spatial limitations and mass resolutions of the simulation zoom simulation (Eckert et al. 2021). Therefore, a sub-grid model is implemented to model the feedback (Barnes et al. 2017; Eckert et al. 2021). The resolution was increased such that in the dark matter only re-simulation the mass of the particles decreased to $m_{DM} = 5.2 \times 10^{9} M_{\odot} h^{-1}$, and in the hydrodynamic re-simulation dark matter particles had mass $m_{DM} = 4.4 \times 10^{9} M_{\odot} h^{-1}$ with gas particle of initial mass $m_{gas} = 8.0 \times 10^{8} M_{\odot} h^{-1}$.

Every cluster selected was also made sure to be void of lower resolution particles within the volume of radius $5R_{200}$ (Barnes et al. 2017). Low resolution particles are normally far away, large particles used to simulate things such as tidal forces from the cosmic web. However, these particles can move following the motion of the universe when simulated to lower redshift, and therefore might cross paths with a galaxy cluster. These low-resolution particles are referenced as type two particles in other sections of this paper. At z=0 the high-resolution region is defined as the spherical volume of radius $5R_{200}$, however, at higher redshift, the high-resolution region is no longer spherical as the particles inside $5R_{200}$ at z=0 come from regions outside as they are attracted gravitationally and tracing them back in time produce a non-spherical region. This makes it more difficult to ensure accurate calculations and results, a method to try to overcome this is described in the next section.

The results analysed from MACSIS use snapshots of the simulation at various redshifts, for example at z = 1 a snapshot is taken in which all data for every particle is saved within this snapshot and later can then be retrieved from the snapshot file.

III. CANDIDATE CATALOGUE

The purpose of the candidate catalogue is to provide a wealth of smaller object data inside galaxy clusters to explore the formation and evolution of galaxy clusters and to calculate properties such as baryon fraction for a range of masses.

The primary candidate for each of the MACSIS clusters is defined as the most massive progenitor derived from the FoF routine, all other FoF haloes are secondary candidates. However, there is an excess of candidates in each cluster, therefore the first selection criteria are the FoF haloes must have $M_{200} \geq 10^{13} M_{\odot}$. The secondary selection criteria require the candidate to not be contaminated. Contaminated means within R_{200}, the candidate is void of particle type twos. These low-resolution particle type twos could affect the analysis of the candidates and are consequently not selected. Now that the candidate selection criteria are defined, all valid candidates in all clusters are added to

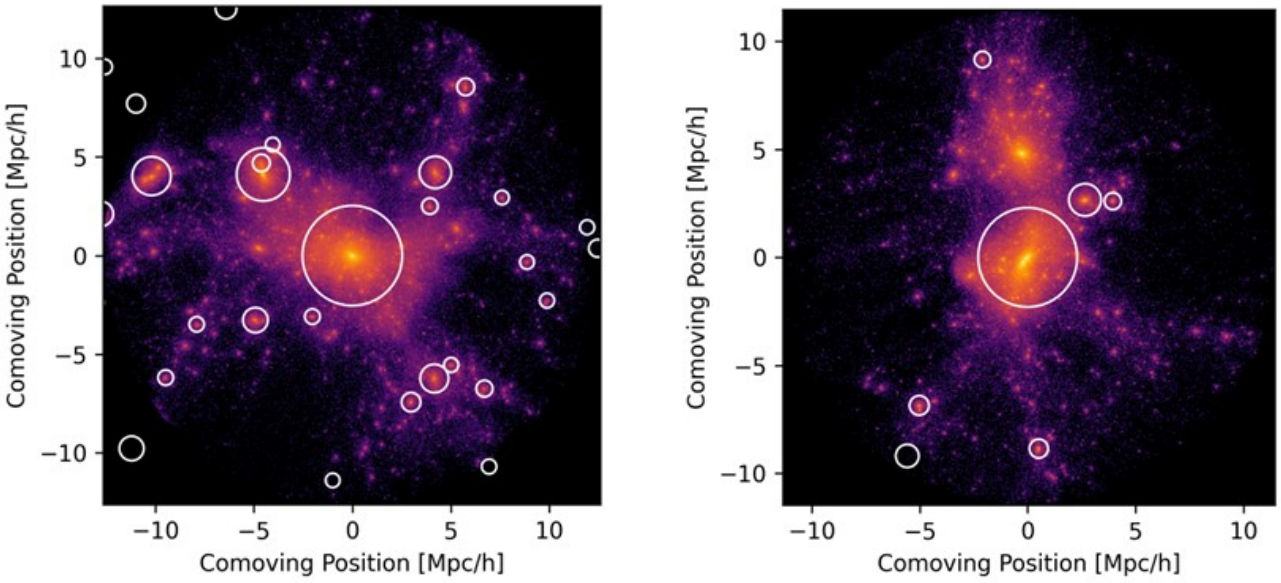

(a) (b)

FIG. 1. Visualisation of candidates in halo region 0 and region 1 for figures 1a and 1b respectively, at Redshift 0. The plots are a heat map of dark matter particles projected in the x-z plane at a distance from the global minimum of potential in co-moving coordinates with a maximum range of $5R_{200}$. The high-density regions mostly represent dark matter haloes of galaxy groups, the high-density regions that are highlighted are valid candidates. The size of the white ring is R_{200} of the candidate it is highlighting. The centre large ring is the primary candidate as it is at coordinates [0,0] and it is the largest ring, R_{200} is proportional to M_{200} and therefore should be the largest ring by definition of the primary candidate. The histogram has been logged to enhance the visual position of the dark matter particles.

a text file for the same redshift. This text file is the candidate catalogue, for each candidate the cluster halo region id, candidate index, M_{200}, R_{200}, coordinates of the centre position in x, y, z, distance to closest particle type 2 in R_{200}, baryon fraction, star fraction and gas fraction are saved. This data is sufficient for this paper's analysis. This candidate catalogue is produced to dramatically reduce time when plotting and calculating values, due to the code not requiring to fetch the data and re-calculate information. Furthermore, this catalogue is the foundation of this project/paper and shall be used for further work.

The halo regions presented in figure 1 show the candidates visually. It is clear that figure 1a has a greater abundance of secondary candidates than figure 1b. However, in both there appear to be large high-density regions of dark matter particles that are not highlighted as valid candidates, these cannot be low mass as they are large and by definition cannot be contaminated if they are inside $5R_{200}$ of the primary candidate at redshift 0 as this is the high-resolution region and therefore void of particle type twos. This can be confirmed by removing the selection criteria and re-plotting. For example in 1b there is a very large high-density region but not highlighted, this is a result of the FoF algorithm as it has connected two of these high-density regions and only highlighted the region with the global minimum of the potential. Moreover, there are valid candidates plotted outside the high-resolution region ($5R_{200}$). This is because we have not set a restriction to how far a candidate can be from the primary candidate, however, in the candidate catalogue we have the coordinates of the centre of each candidate and can calculate the distance and remove it if necessary. However, at higher redshift, the high-resolution region is no longer spherical, so as a result of this all valid candidates at any distance are kept.

The MACSIS simulation is not perfect and the physics models simulated can act not as intended. Using figure 2, 13 unique cluster outliers can be identified, highlighted and removed from the catalogue. These outliers could be due to a problem with the simulated feedback in the cluster, where too many baryons escape the halo and are not recovered. The catalogue now consists of candidates from 377 unique galaxy clusters.

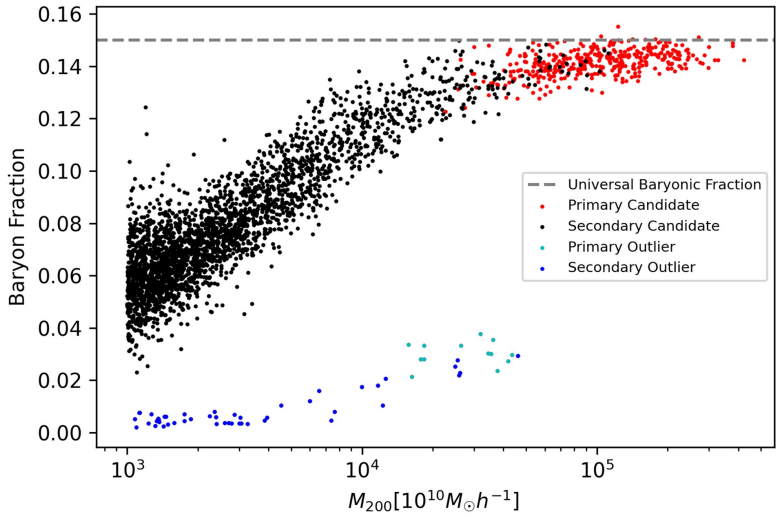

FIG. 2. Baryon fraction plot for all candidates masses from the 390 MACSIS clusters at redshift 0. The baryon fraction is calculated from all particles within R_{200} of each candidate. All secondary candidate outliers come from the 13 primary candidate outliers.

IV. RESULTS

Maybe include 4 pics in a grid of DM mass maps to show evolution (with rings?)

A large portion of this project was creating the candidate catalogue and evolving it to include all useful information that future work may require. The results provided in this section are mostly a product of this catalogue. We performed our analysis at z = 0.0, 0.46, 1.0, 1.56, 2.05, 2.69, and 3.08. Our methodology was to start at z = 0 for most parts of the project we thought of analysing, and then extend them all using a script to higher redshift.

I wrote the code to produce the candidate catalogue for every redshift. My project partner Aaron focused on candidate statistics, he wrote the code to produce the probability figure 3 which I slightly adapted to get adjusted figures, fixing the scales at a set size for example and adapted to produce the two plots in figure 4 to summarize his work. I also did some work on candidate statistics, making figure 5. The majority of my work, aside from the catalogue, was working on mass fractions, particularly the baryon fraction. My code produced every plot apart from figure 3, as already discussed, and figure 1 in which I only contributed by writing code to plot the candidate rings.

A. Candidate Statistics

Candidate statistics is the method of using secondary candidates, from the catalogue, to represent smaller objects within the galaxy cluster and track their position and mass during redshift evolution to probe for clues of galaxy formation, such as the hierarchical model where smaller objects (secondary candidates) collapse and merge to give rise to larger objects.

Using figure 3, the spread of secondary candidate mass can be visually seen decreasing, contrasting the distance to the primary candidate increasing with increasing redshift. Figure 4 is used to represent the plots in figure 3 in a more summarized, analytical way to directly compare every redshift. In the Λ-cold dark matter model, galaxy cluster formation is hierarchical. Using figure 4, secondary candidates representing smaller galaxy structures are getting, on average, closer to the centre. This can be described by the gravitational attraction of the galaxy cluster centre attracting smaller structures. The increasing mass with redshift can be explained by mergers of smaller structures with each other. The standard deviation of the distance also increases with redshift, meaning smaller structures are more localised, this can be due to the gravitational collapse and merging of smaller structures with each other as well, as they make their way to the cluster centre, which can be validated by both the mean values in each plot. The standard deviation in the mass plot significantly decreases with redshift. Using this and everything just discussed, a theory of the structure formation of a galaxy cluster can be built. At the early stages of a galaxy cluster's life, there are many low mass small structures which are quite spread out. Due to gravity, the structures start to fall down to the cluster centre and collapse and merge with each other, decreasing the mean distance to the centre and the

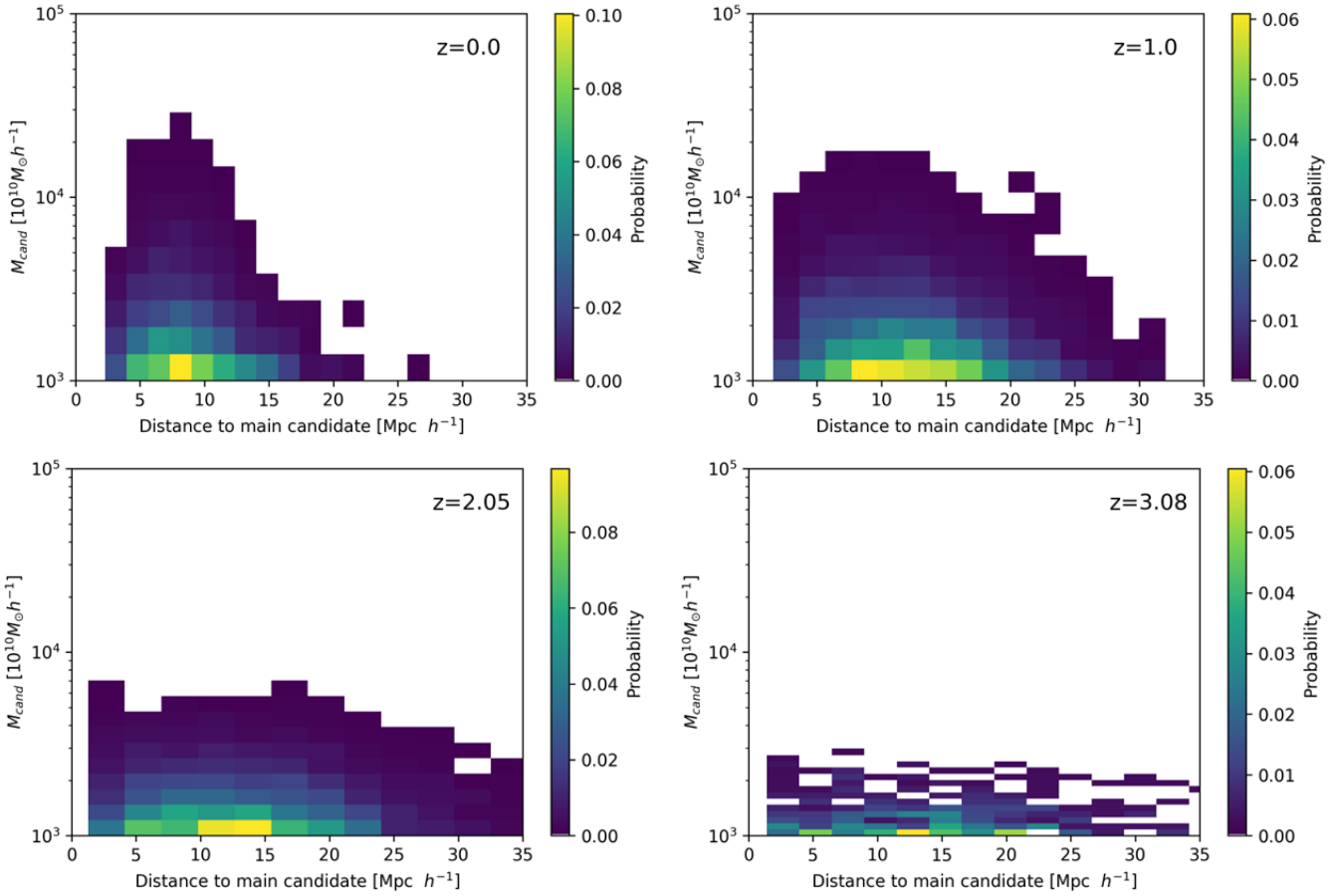

FIG. 3. The redshift evolution of the probability of the secondary function as a function of its own mass and the distance to the primary candidate. The colour map as shown on the plots indicates the highest probability to find a secondary candidate with a certain mass and how far out it is from the primary candidate. The redshift is indicated at the top right of each plot. The secondary candidates used is a combination of all 377 MACSIS clusters.

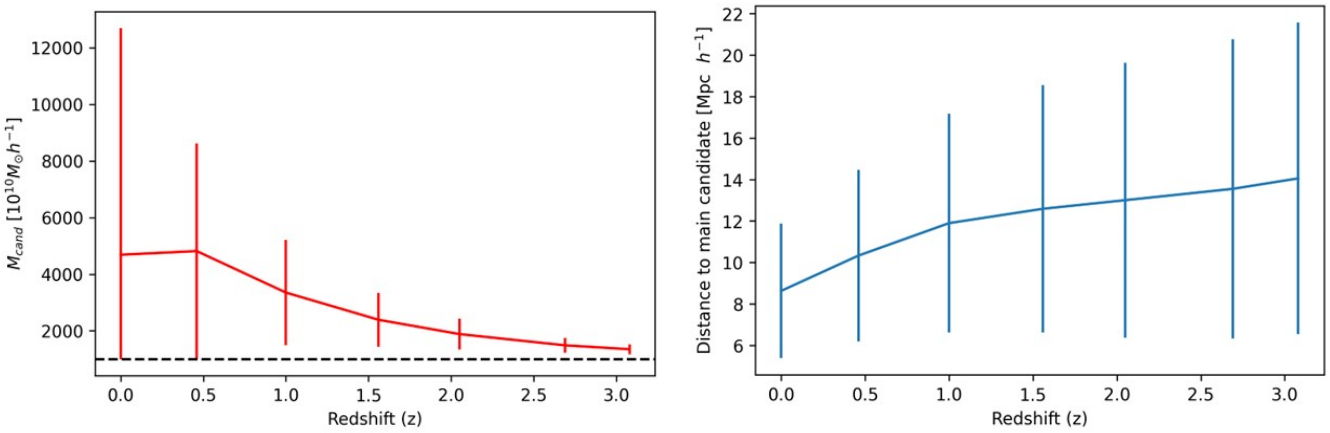

FIG. 4. The redshift evolution of secondary candidate mass (left) and secondary candidate distance to the primary candidate (right). The mean of secondary candidate mass and distance were plotted, and the error bars on each plot are the standard deviation. However, for the mass plot the error bars are plotted asymmetric due to the constraint on the secondary candidate mass by the selection criteria described in the candidate catalogue section, this is shown by the black dotted line.

overall distribution as well as simultaneously increasing the mean mass. As some won't merge with each other, the

distribution of masses starts to increase. This mechanism carries on with time, with distance steadily decreasing and mass increasing. However, between z = 0 and 0.5 the mean mass stays roughly constant, but the distribution still increases significantly. This suggests that mergers are still occurring, specifically with the secondary candidates that have already merged a few times and now have significant mass to have a big gravitational pull of its own to keep increasing mass at a faster rate, but there is still a significant number of low mass small structures present. These findings correlate with a hierarchical model of galaxy cluster formation and evolution, as described in section (II A 2).

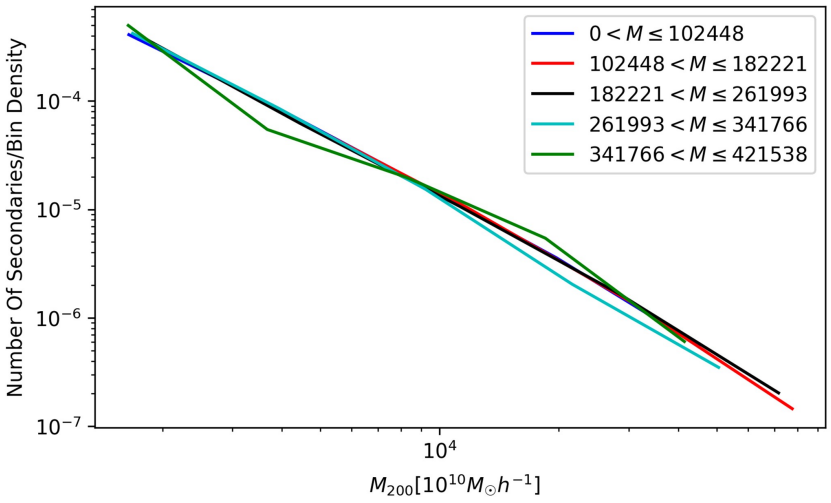

FIG. 5. The mass and number of secondary candidates dependency on the primary candidate mass at z = 0. The primary candidates are split into 5 equally spaced bins, for the primaries in each bin all their secondary candidates' masses (M_{200}) were then logarithmically binned and plotted. The legend represents the primary mass M (M_{200}) and the boundaries of each bin and their respective colour.

Figure 5 suggests there is no correlation between the primary candidate mass at the centre of the cluster and the number or mass of the secondary candidates, representing the smaller structures surrounding the centre at z = 0. For all masses of secondary candidates, all primary candidates have roughly the same number of them, with there being no difference with increased primary candidate mass. Furthermore, each primary mass bin has roughly the same range of secondary candidate masses. This implies all galaxy clusters at z = 0, independent of mass, evolved to have a similar structure beyond the primary candidate.

B. Baryon Mass Fraction

Massive galaxy clusters cover a large region of the universe and subsequently are representative of the mean matter content of the universe, and therefore the baryon fraction (Rasheed et al. 2011). The deep potential of massive galaxy clusters also reduces the impact of non-gravitational processes, further making them a better choice for analysing cosmological properties such as the baryon fraction (Barnes et al. 2017). Real-world observations of galaxy clusters reveal a depletion of baryons compared to the universal baryon fraction (Rasheed et al. 2011), $\overline{f_b} = \frac{\Omega_b}{\Omega_m} = \frac{0.04825}{0.307} = 0.157$. Observations of quasars also state that at z = 0, almost half of the baryons are unaccounted for in the universe. It is thought this is due to difficulty observing a range of temperatures, but at z$\sim$ 3 the majority of baryons can be accounted for (Houjun Mo et al. 2010). These scenarios of missing baryons are the chosen paths to explore in this section.

The baryon fraction, and its components, are displayed for all gas and just hot gas in figures 6 and 7 respectively. The mass fractions are calculated by summing up the masses of all the particles just within R_{200} of each candidate. In MACSIS the two particles that make up the baryonic matter are stars and gas, shown by equations 2 and 3 for total and hot baryon fractions respectively.

The trends of figures 6 and 7 show the increase of baryon and gas fraction with candidate mass. The primary candidates, the most massive progenitors, have the highest baryon fractions with secondary candidates trailing off with decreasing baryon fraction and decreasing mass. By binning the mass bins logarithmically and plotting the median mass fraction and standard deviation in each bin we can validate the continuation of the trend between the secondary and primary candidates. Therefore, we can treat the primary and secondary candidates as a combined set

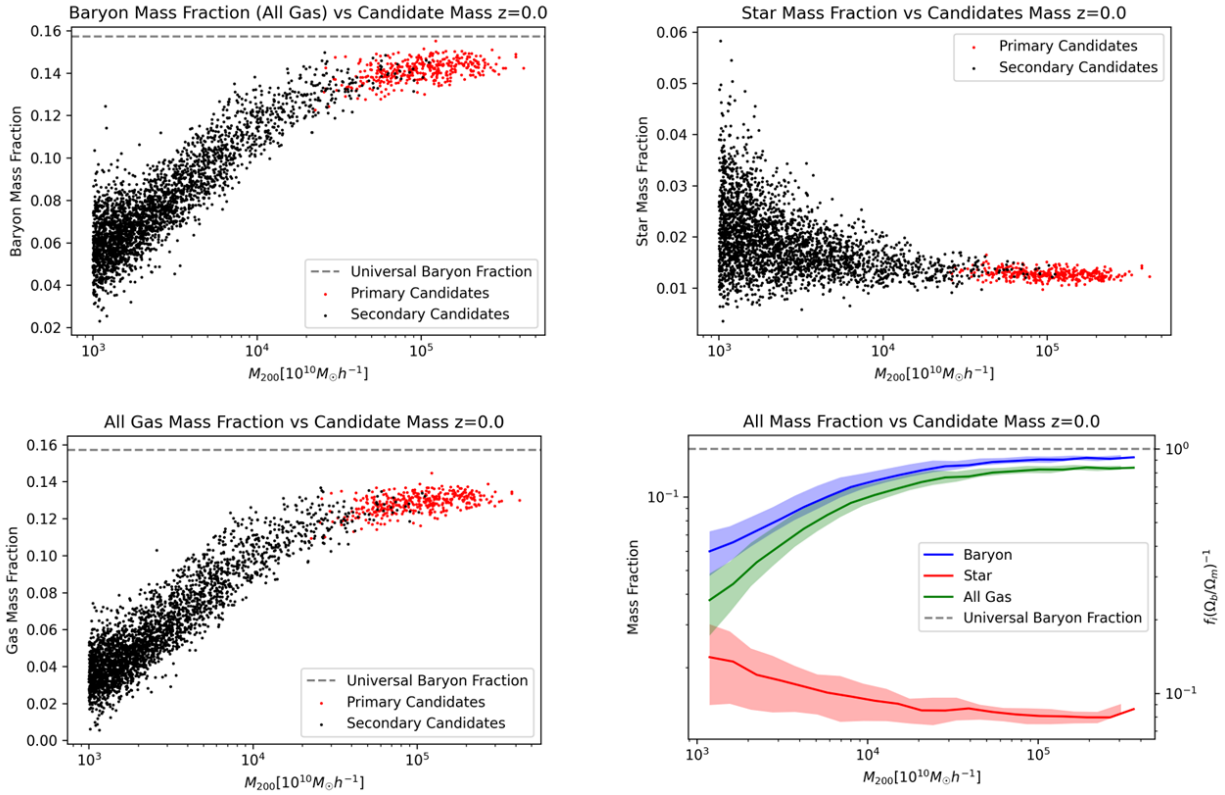

FIG. 6. Baryon, all gas and star mass fractions plotted independently versus candidate mass, for every secondary candidate (black) and primary candidate (red) from all 377 MACSIS clusters at z = 0. The baryon fraction is calculated using equation 2. The dashed grey line represents the universal baryon fraction $\overline{f_b} = \frac{\Omega_b}{\Omega_m} = 0.157$. The overall plot (bottom right) includes the standard deviation of each mass fraction as shown by the lightly shaded region. The right axis represents the fraction of the universal baryon fraction each component makes up, where $i = baryon, gas, star$.

as done in the combined plots. The increase of baryon and gas fraction with mass can be explained by the containment of baryon matter being pushed out by astrophysical processes, discussed in section (II A 1), by the deeper gravitational potential well of higher mass candidates. As primary candidates, by definition, are the most massive progenitor they would be expected to retain the most baryon content under this ideology, and they do.

Figure 7 displays all the mass fractions containing just hot gas. The threshold used to just select hot gas particles was a temperature of $\geq 10^6 K$, this value was used to represent the gas that produces X-ray emission to more directly compare to observational results in the real world. The primary difference between all gas and just hot gas is seen in the low candidate mass region ($\leq 10^{14} M_\odot h^{-1}$) where the baryon and gas fraction significantly decreases, the baryon and gas fraction of the primary candidates and high mass secondary candidates remain unchanged. This means that lower mass candidates are the primary holders of cold gas in galaxy clusters. Furthermore, candidates with mass $\sim 10^{13} M_\odot h^{-1}$ almost just consist of cold gas as some have a gas fraction of 0. This could be explained by lower mass candidates being new and young systems in the galaxy cluster, which are far away from the centre and are yet to merge with other candidates and don't get affected by the processes from the high-density cluster centre so the gas stays relatively cool. Whereas higher mass candidates have undergone many mergers that have heated up the gas, as well as being under influence of processes from the high-density environment as they might have drifted closer to the centre. As low mass candidates have the majority of cold gas, they would be expected to have a lot more star formation. This is confirmed by the star fraction plot of figures 6 and 7, which show significantly greater star fraction towards the lower candidate mass range.

Extending the z = 0 baryon fraction analysis to higher redshift produces figure 8. The mean total baryon fraction can visibly be seen to decrease with decreasing redshift. This decrease is essentially due to dark matter being easier to re-accrete back into the cluster haloes than baryons are. Essentially, this is the nature of gas being dissipative and dark matter being dissipationless. More specifically, as haloes gain more mass, the temperature at R_{200} increases causing the gas to be shock-heated and slows down the accretion process into the halo. In addition, during the formation of haloes, mergers and accretion can expel some dark matter and baryons. But as just mentioned, dark matter is

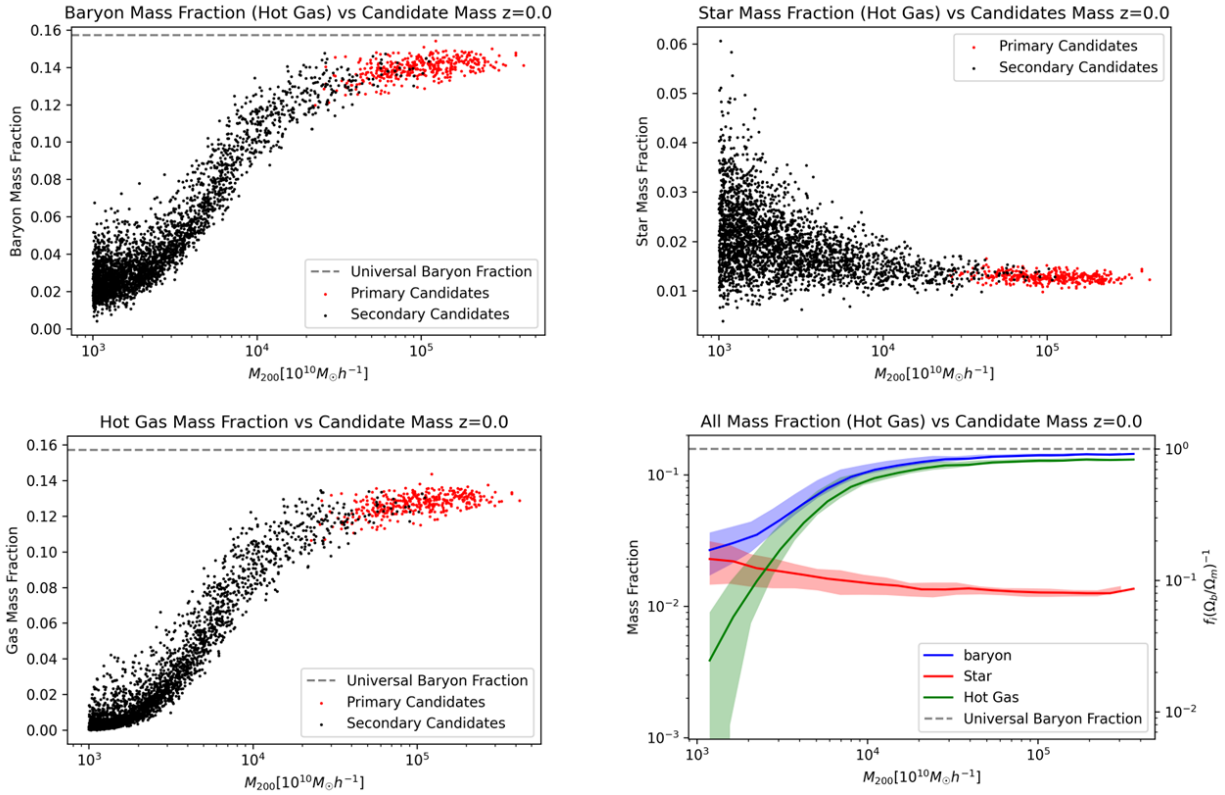

FIG. 7. Baryon, hot gas and star mass fractions plotted independently versus candidate mass, for every secondary candidate (black) and primary candidate (red) from all 377 MACSIS clusters at z = 0. The baryon fraction is calculated using equation 3. The dashed grey line represents the universal baryon fraction $\overline{f_b} = \frac{\Omega_b}{\Omega_m} = 0.157$. The overall plot (bottom right) includes the standard deviation of each mass fraction as shown by the lightly shaded region. The right axis represents the fraction of the universal baryon fraction each component makes up, where $i = baryon, gas, star$.

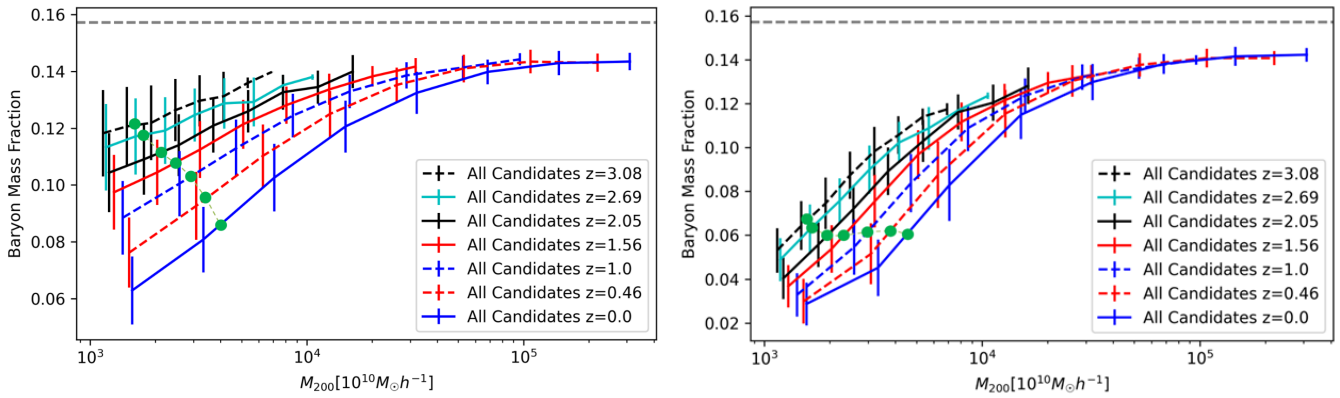

FIG. 8. Hot baryon fraction (right) and baryon fraction (left) plots against candidate masses for a range of redshifts. The green dots on every redshift line represent the mean baryon fraction for that redshift. All baryon fractions for every candidate in each redshift were logarithmically binned by mass, then the median and standard deviation were plotted at the centre of each bin. The dashed line represents the universal baryon fraction, $\overline{f_b} = \frac{\Omega_b}{\Omega_m}$.

re-accreted easier which even further decreases the baryon fraction inside R_{200} (increases denominator of equation 2) and the gas (WHIM) around gains baryons. Furthermore, many baryons do not collapse into the haloes and stay in the WHIM (Peirani et al. 2012). Figure 8 loosely agrees with this book, Houjun Mo et al. 2010, where observational data inferred from quasars conclude that at z = 0 half of baryons are missing, however, at z = 3 most baryons can be accounted for in the universe, but galaxy clusters should be representative of the mean matter content on the universe

so the same trend should be seen in MACSIS. At z = 0, the mean baryon fraction is roughly 55 percent and at z = 3, the mean baryon fraction increases to around 80 percent. This increase is significant, but at z = 3 a few baryons are still unaccounted for. Further investigation into this is carried out with figure 11.

The average hot baryon fraction in figure 8 (right) stays roughly constant, and at all times is lower than the total baryon fraction. This would suggest that cold gas is responsible for the decrease in baryon fraction, as just hot gas produces a constant value of the mean baryon fraction. At higher redshift low mass candidates contain a lot more cold gas, the baryon fraction of low mass candidates drops around 50 percent compared to the total baryon fraction. High mass candidates, comparatively, do not decrease in baryon fraction when just selecting hot gas, meaning they mostly consist of hot gas. This would further suggest that when measuring the baryon fraction of galaxy clusters observationally, there will be very little if not any change at redshifts up to z = 3. This agrees with this paper, Chiu et al. 2018, where observationally they state the baryon content of clusters at a fixed mass basically does not change over roughly $9Gyr$. Note, z = 3 equals around $11.5Gyr$, so the paper does not cover the exact same redshift range, but our results are consistent up until that point.

Primary candidate baryon fraction increases at lower redshift, this is due to the primary candidate gaining more mass over time and therefore a deeper potential well to stop losing as many baryons by feedback processes. At higher redshifts, primary candidates had a broader range of masses and were more overlapped with secondary candidates. To further explore this idea of redshift evolution of baryon fraction on different mass candidates/objects, the candidates were split into different mass bins.

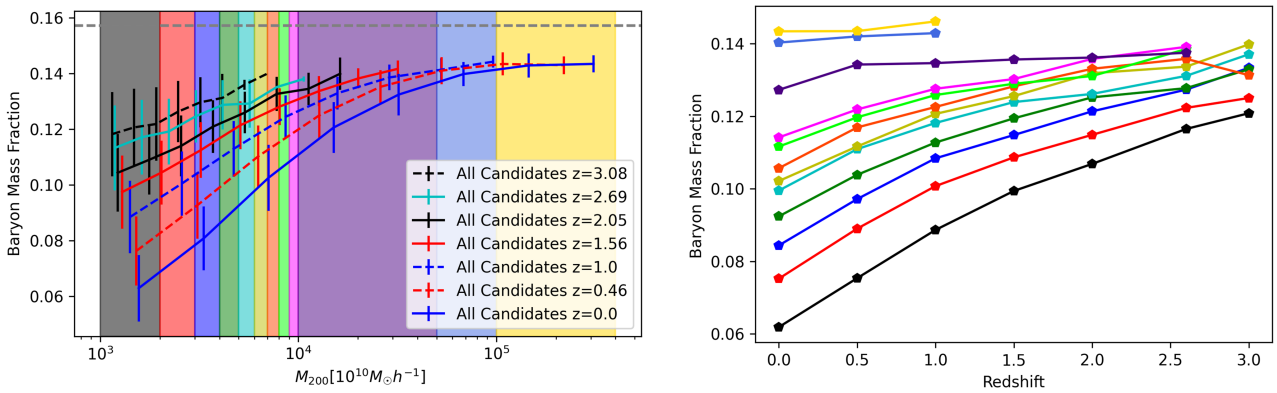

FIG. 9. The redshift evolution of baryon fraction for intervals of candidates masses. Using the baryon fraction plot from figure 8, mass bins were placed and the baryon fraction of all candidates in each bin was averaged for every redshift and then plotted on the right. For example, the most left black bin represents the range $10^{13} - 11^{13} M_\odot h^{-1}$, using the plot on the left the average baryon fraction as taken inside the bin at each redshift. This averaged baryon fraction for that mass range is then plotted on the right as baryon fraction vs redshift. Not all mass bins have the same width, at the higher mass range the bins were widened to reduce clutter on the right plot as from bin to bin there is not as much variety as the low end mass spectrum. The grey dashed line represents the universal baryon fraction, $\overline{f_b} = \frac{\Omega_b}{\Omega_m}$.

To investigate and compare the redshift evolution of baryon fraction for different candidate masses, figure 9 (left) was used to place mass bins covering a range of redshifts to produce figure 9 (right). The decrease of baryon fraction is clearly more rapid for less massive objects. The lowest mass bin, covering the range $10^{13} - 11^{13} M_\odot h^{-1}$, has the greatest decrease in baryon fraction by roughly 50 percent, from $f_b \sim 0.12$ to 0.6. The percentage lost for increasing redshift decreases for each mass bin. For the most massive candidates, the baryon fraction is almost constant. These mass dependent results agree with this recent paper, Angelinelli et al. 2022, which used a set of large galaxy clusters from the *Magneticum* simulation. They also conclude that the baryon fraction decreases with redshift, shown in figure 8 and that the decrease for lower mass objects is much greater than high mass objects inside central regions of galaxy clusters.

Continuing on from the analysis conducted in figure 8 where we compared the difference of hot gas baryon fraction and the total baryon fraction, alongside figure 9 where we compared the baryon fraction for different mass candidates, both with the decrease of redshift. To summarise both of these aspects into one, figure 10 was produced. It represents the missing baryon fraction divided by the total baryon fraction for similar mass candidates, using the same mass bins as figure 9. This is the fraction of baryons an observer would theoretically miss when conducting an X-ray observation of galaxy clusters for different candidate masses. In equation form:

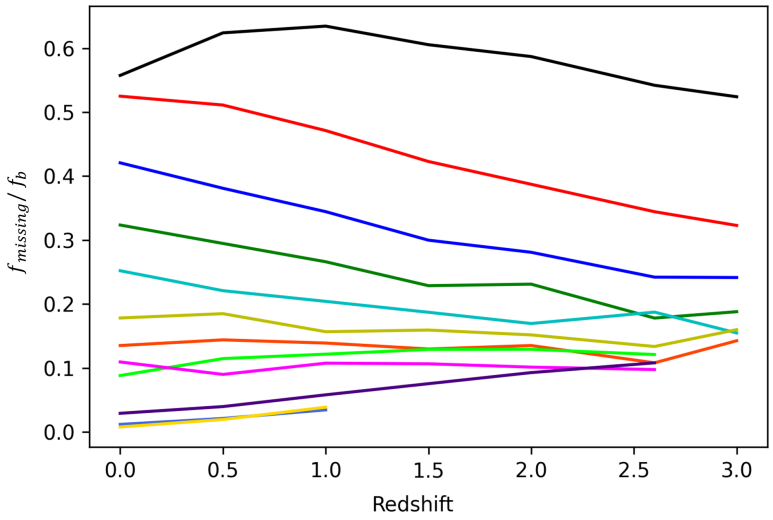

FIG. 10. Redshift evolution of the missing baryon fraction divided by the baryon fraction from z = 0 to z = 3. This plot utilises the same mass bins from figure 8 therefore, the coloured lines represent the same objects within the bin width. The missing baryon fraction divided by the baryon fraction tries to evaluate the fraction of baryons 'missed' when observing a real galaxy cluster due to temperature issues.

$$\frac{f_{missing}}{f_b} = 1 - \frac{f_{obvs}}{f_b}, \tag{4}$$

where $f_{missing} = \frac{M_{gas}(\leq 10^6 K)}{M_{200}}$: the fraction of cold gas, $f_{obvs} = f_{b,hot}$ as shown in equation 3: the observed X-ray emitted hot gas baryon fraction and f_b is the total baryon fraction of both hot and cold gas, equation 2. f_{obvs} and f_b are both extracted from figure 9.

In figure 10, a correlation between candidate mass and the missing baryon fraction can be seen. The lower the candidate mass, the more baryon content cannot be observed. Very high mass ($\geq 10^{15} M_\odot h^{-1}$) candidates have basically no missing baryons at z = 0. Candidates below $10^{14} M_\odot h^{-1}$ all have a general trend of increase of missing baryons with the decreasing of redshift. Candidates of high mass above $10^{14} M_\odot h^{-1}$ have a very slight decrease in missing baryons as redshift decreases. As z increases, R_{200} decreases resulting in a more dense region, the universe was denser in the past and therefore required an even more dense region to allow collapse, denser regions are hotter and therefore the missing baryon fraction goes down as a higher fraction of gas emits X-rays. This is true for a gravity-only model, however, feedback and gas-cooling processes change the temperature distribution. We can see for low mass candidates the gravity-only model is suitable, but for more massive candidates such as primaries in the middle of the cluster, in a much denser environment, feedback cancels out the result of the gravity-only model.

Throughout the project, it was obvious that higher mass candidates had the greatest baryon fraction, as shown in figures 6 and 8. However, the baryon fraction of even the most massive candidates still don't equal the universal baryon fraction. This discrepancy is around 10 percent using figures 8 and 11. This is due to baryons laying on the outskirts of candidate haloes (Rasheed et al. 2011; Peirani et al. 2012). The processes that are responsible are discussed in subsection (II A 1) and already in the results when analysing the decrease of baryon fraction for the decrease in redshift displayed in figure 8. One process responsible is the gas being shock-heated (Rasheed et al. 2011; Peirani et al. 2012). Figure 11 agrees with the results and theory concluded in Rasheed et al. 2011; Peirani et al. 2012. The total baryon fraction, at z = 0, increases towards the universal baryon fraction at larger radii. At $5R_{200}$ the baryon fraction increases to $f_b = 0.156$, this is now only about 1 percent off the universal baryon fraction.

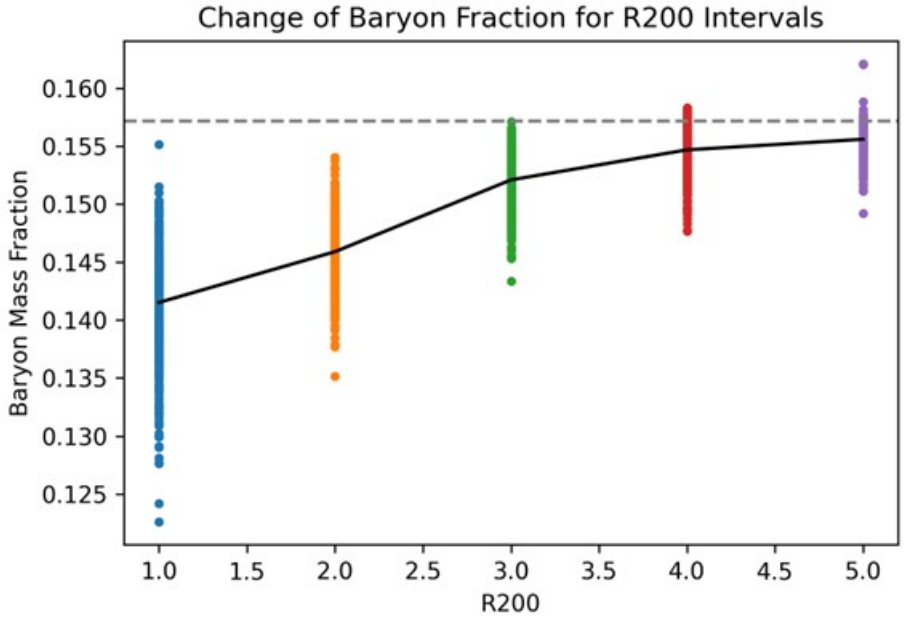

FIG. 11. The baryon fraction of primary candidates at increasing radii at z = 0. The black line is the medium baryon fraction at every radii interval. Each coloured circle represents the baryon fraction of a candidate, calculated within their respective radius. Throughout the paper, the baryon fraction was calculated within the virial radius, R_{200}. Analysis of all candidates, and specifically the most massive candidates, provided a baryon fraction below the universal fraction, displayed in this plot as the grey dashed line. This plot extends the radius of where the baryon fraction is calculated, in steps of one R_{200} out to $5R200$ at the edge of the high-resolution region.

V. CONCLUSION

Massive galaxy clusters from MACSIS hydrodynamical, baryonic, and N-body simulations (Barnes et al. 2017) were used to study galaxy cluster formation and the redshift evolution of the baryon fraction. The redshift values used were z=0.0, 0.46, 1.0, 1.56, 2.05, 2.69, and 3.08. Candidates for analysis were chosen from the FoF haloes for all 377 MACSIS clusters at every redshift step. The criteria for selection was a lower limit on mass ($\geq 10^{13} M_{\odot} h^{-1}$) and for no low-resolution particles to be within R_{200} of the candidate. A candidate catalogue for every redshift step was created at the beginning of the project to allow our analysis of a range of different mass objects inside the galaxy cluster. Primary candidates are the most massive progenitor of each cluster, where each zoom simulation is centred on. Secondary candidates are all other identified dark matter haloes by the FoF algorithm, figure 1 highlights the candidates in two separate clusters. The candidate catalogue creation was an important part of the project and took some considerable time to code, it allowed the majority of the work in the project to be carried out and provides a good base of information for future work to do with MACSIS clusters. Our main results for galaxy cluster formation, using candidate statistics are:

- As shown in figure 3 and summarized in figure 4, secondary candidates increase in mass and get closer to the primary candidate with the decrease of redshift. The smaller objects (secondary candidates) merge with other small objects, increasing in mass, whilst simultaneously being attracted to the cluster centre by gravity. This behaviour of smaller objects is in agreement with what is expected from the currently-agreed cosmological model, the ΛCDM model, which includes a hierarchical structure formation mechanism. The distribution of smaller object mass also increases significantly with decreasing redshift, contrasting the decreasing distance distribution. This suggests that smaller objects become more localised together, closer to the primary candidate whilst there being much more variety in their mass.

- There is no correlation between the number and mass of secondary candidates and primary candidate mass at z = 0 (see figure 5). This would imply that all galaxy clusters evolve to current redshift with the same structure outside the primary candidate, independent of cluster mass. It could be that smaller objects follow similar or proportional 'paths' when collapsing into the different mass primary candidates, to accrete the same mass and keep the same relative abundance.

This section's results show that the MACSIS simulations successfully simulate the hierarchical structure formation of massive galaxy clusters, by representing smaller objects in the cluster as secondary candidates and tracking their position and mass at different redshifts. We also produce some interesting results, that the mass of the primary cluster, and at extension the cluster, has no impact on the number or mass of smaller objects surrounding the primary candidate. Intuitively I would think more massive primary candidates would be surrounded by higher mass candidates.

Massive galaxy clusters are representative of the mean matter content of the universe, and therefore, representative of the universal baryon fraction (Rasheed et al. 2011), which in MACSIS is $\overline{f_b} = \frac{\Omega_b}{\Omega_m} = 0.157$. The total baryon fraction and the hot ($\geq 10^6 K$) baryon fraction are calculated using equation 2 and 3, respectively. The hot gas baryon fraction is used to represent the observational baryonic matter as hot gas emits X-rays. The results for the redshift of the baryon fraction are as follows:

- The baryon fraction of candidates strongly depends on candidate mass for z = 0 (see figures 6, 7). The deeper potential wells of greater mass candidates retain more baryons being ejected by mergers and feedback processes out of the halo. Using the same figures the difference between all and hot gas can be determined to only significantly decrease the baryonic fraction for candidates $\leq 10^{14} M_{\odot} h^{-1}$, inferring they mostly consist of cold gas. This is backed up by having the highest star formation, as shown in figures 6, 7.

- The mean total baryon fraction from z = 3 to z = 0 decreases and the hot baryon fraction is constant with redshift in the same range (see figure 8, left and right respectively). The total baryon fraction is somewhat with observational data, with roughly half of baryons being unaccounted for at z = 0 and the majority of baryons can be accounted for at z = 3. Results agree at lower redshift at around 50 percent, but at z = 3 still, only 80 percent of barons are accounted for. The hot baryonic fraction agrees with the limited observational data with it being constant, data only goes up to z = 1.25, but is consistent up to then.

- The decrease of baryon fraction is more rapid for less massive objects in galaxy clusters. Our lowest mass candidates ($\sim 10^{13} M_{\odot} h^{-1}$) lost 50 percent of their baryonic fraction with decreasing redshift, whilst the most massive candidates ($\sim 10^{15} M_{\odot} h^{-1}$) have an almost constant baryonic fraction. This is an agreement from a paper based on a different massive cluster simulation.

- The theoretical fraction of the baryonic fraction missed due to non-X-ray emitting cold gas. As expected, due to the hot baryon fraction figure 7, lower mass candidates have a much greater fraction missing observationally (see figure 10) due to the high content of cold gas. The lowest mass candidates ($\sim 10^{13} M_{\odot} h^{-1}$) have roughly 60 percent of their baryons 'missing', the most massive candidates ($\sim 10^{15} M_{\odot} h^{-1}$) have little to no fraction missing, especially at z = 0.

- The rest of the baryons of primary candidates are on the outskirts of the halo (see figure 11). For every increase in radius, from within all particles summed mass was calculated, and the baryon fraction increases consistently. This was investigated due to even the most massive candidates not containing the universal baryon content, as shown in an earlier figure 9. This correlation of baryon fraction and radius agrees with observational results and theory.

Our results, in general, were very successful with other reliable observational data and simulations. If some results couldn't be backed up by observational data, they could be mostly explained by well reconsigned theories in astronomy. Therefore, MACSIS provides the opportunity to analyse the most massive, realistic galaxy clusters possible via the ΛCDM model. It allows the chance to produce robust predictions at high redshift for future observational projects.

VI. FUTURE WORK

The secondary dependency on primary mass (figure 5) could be extended to higher redshift to study if there is a change to this interesting result. Figure 11 only includes primary candidates, and not all candidates from the candidate catalogue, because when extending the radius for baryon fractions calculations of candidates all of them with a range of $5R_{200}$ would reach outside the high-resolution region. A method of checking how far the secondary candidate is and extending the radius to its maximum value inside the high-resolution region could be made to further the correlation between candidate baryon fraction and radii for different mass candidates.

A fundamental change could be made to the process of selecting the primary candidate, instead of just using the first item in the FoF halo list. This change would consist of tracking the primary from z = 0 to small redshift intervals, we would then assume the minimum displacement of the centre of the primary candidate from one redshift to another

is the primary candidate. Using the current method is not a perfect solution, as sometimes the FoF algorithm jumps to a different high mass candidate, this will induce some error in our results.

Next semester, some improvements as just mentioned can be made, alongside a new focus on protoclusters. Protoclusters are very high redshift galaxy clusters.

REFERENCES

Anderhalden, Donnino and Juerg Diemand (2013). "Density profiles of CDM microhalos and their implications for annihilation boost factors". In: *Journal of Cosmology and Astroparticle Physics* 2013.04, pp. 009–009.

Angelinelli, M. et al. (2022). "Mapping 'out-of-the-box' the properties of the baryons in massive halos". In: *Astronomy &amp Astrophysics* 663, p. L6.

Bahcall, Neta A. (1996). *Clusters and superclusters of galaxies*.

Barnes, David J. et al. (2017). "The redshift evolution of massive galaxy clusters in the MACSIS simulations". In: *MNRAS* 465 (1), pp. 213–233.

Bond, J. Richard, Lev Kofman, and Dmitry Pogosyan (1996). "How filaments of galaxies are woven into the cosmic web". In: *Nature* 380 (6575), pp. 603–606.

Bufanda, E. et al. (2016). "The evolution of active galactic nuclei in clusters of galaxies from the Dark Energy Survey". In: *Monthly Notices of the Royal Astronomical Society* 465.3, pp. 2531–2539.

Chandra X-ray observatory (2012). *Groups and Clusters of Galaxies*. `https://chandra.harvard.edu/xray_sources/galaxy_clusters.html`.

Chiu, I et al. (2018). "Baryon content in a sample of 91 galaxy clusters selected by the South Pole Telescope at 0.2 &ltz &lt 1.25". In: *Monthly Notices of the Royal Astronomical Society* 478.3, pp. 3072–3099.

Davis, Marc et al. (1985). "THE EVOLUTION OF LARGE-SCALE STRUCTURE IN A UNIVERSE DOMINATED BY COLD DARK MATTER". In: *The Astrophysical Journal* 292, pp. 371–394.

Diemand, Jürg and Ben Moore (2011). "The Structure and Evolution of Cold Dark Matter Halos". In: *Advanced Science Letters* 4.2, pp. 297–310.

Eckert, Dominique et al. (2021). "Feedback from Active Galactic Nuclei in Galaxy Groups". In: *Universe* 7.5, p. 142.

Efstathiou, G. et al. (1988). "Gravitational clustering from scale-free initial conditions". In: *MNRAS* 235 (3), pp. 715–748.

Ellis, George F. R. (2006). *Issues in the Philosophy of Cosmology*.

Gorenstein, Paul and Wallace Tucker (1978). "Rich Clusters of Galaxies". In: *SCIENTIFIC AMERICAN INC* 239.5, pp. 110–131.

Houjun Mo, von, Frank van den Bosch, and Simon White (2010). *Galaxy Formation and Evolution*. Cambridge University Press.

Huss, A., B. Jain, and M. Steinmetz (1999). "The formation and evolution of clusters of galaxies in different cosmogonies". In: *MNRAS* 308.4, pp. 1011–1031.

Jungman, Gerard, Marc Kamionkowski, and Kim Griest (1996). "Supersymmetric dark matter". In: *Physics Reports* 267.5-6, pp. 195–373.

Kaastra, J. S. et al. (2008). "Clusters of Galaxies: Beyond the Thermal View". In: *Space Science Reviews* 134, pp. 1–6.

Lisa Germany et al. (1999). *Intra-cluster medium*. `https://astronomy.swin.edu.au/cosmos/`.

More, Surhud et al. (2011). "THE OVERDENSITY AND MASSES OF THE FRIENDS-OF-FRIENDS HALOS AND UNIVERSALITY OF HALO MASS FUNCTION". In: *The Astrophysical Journal* 195.1.

Mushotzky, Richard (1998). "X-ray emission from clusters and groups ofgalaxies". In: *Proceedings of the National Academy of Sciences* 95.1, pp. 72–77.

Padovani, P. et al. (2017). "Active galactic nuclei: what's in a name?" In: *The Astronomy and Astrophysics Review* 25.1.

Peirani, Sébastien et al. (2012). "Evolution of the baryon fraction in the Local Group: accretion versus feedback at low and high z". In: *Monthly Notices of the Royal Astronomical Society* 427.3, pp. 2625–2635.

Rasheed, Bilhuda, Neta Bahcall, and Paul Bode (2011). "Searching for the missing baryons in clusters". In: *Proceedings of the National Academy of Sciences of the United States of America* 108 (9), pp. 3487–3492.

Sarazin, Craig L. (1988). *X-RAY EMISSION FROM CLUSTERS OF GALAXIES*. Cambridge University Press, p. 252.

Taylor, James E. (2011). "Dark Matter Halos from the Inside Out". In: *Advances in Astronomy* 2011, pp. 1–17.

Vikhlinin, A A et al. (Apr. 2014). "Clusters of galaxies". In: *Physics-Uspekhi* 57.4, p. 317.

White, Simon DM and Carlos S Frenk (1991). "Galaxy formation through hierarchical clustering". In: *The Astrophysical Journal* 379, pp. 52–79.